

Monodisperse Nanocrystal Superparticles through a Source-Sink Emulsion System

*Emanuele Marino (ORCID: 0000-0002-0793-9796),¹ Sjoerd W. van Dongen (ORCID: 0000-0003-3617-5614),^{1,4} Steven J. Neuhaus (ORCID: 0000-0002-6754-1165),² Weixingyue Li (ORCID: 0000-0003-0001-6371),¹ Austin W. Keller (ORCID: 0000-0003-1288-7027),² Cherie R. Kagan (ORCID: 0000-0001-6540-2009),^{1,2,3} Thomas E. Kodger (ORCID: 0000-0002-7796-9165),⁴ Christopher B. Murray (ORCID: 0000-0002-3491-122X)^{1,2, *}*

¹Department of Chemistry, ²Department of Materials Science and Engineering, ³Department of Electrical and Systems Engineering, University of Pennsylvania. Philadelphia, Pennsylvania, 19104, United States.

⁴Physical Chemistry and Soft Matter, Wageningen University and Research, 6708WE, Wageningen, The Netherlands.

ABSTRACT: Superparticles made from colloidal nanocrystals have recently shown great promise in bridging the nanoscale and mesoscale, building artificial materials with properties designed from the bottom-up. As these properties depend on the dimension of the superparticle, there is a need for a general method to produce monodisperse nanocrystal superparticles. Here, we demonstrate an approach that readily yields spherical nanocrystal superparticles with a polydispersity as low as 2%. This method relies on the controlled densification of the nanocrystal-containing “source” emulsion by the swelling of a secondary “sink” emulsion. We show that this

strategy is general and rapid, yielding monodisperse superparticles with controllable sizes and morphologies, including core/shell structures, within a few minutes. The superparticles show a high optical quality that results in lasing through the whispering gallery modes of the spherical structure, with an average quality factor of 1600. Assembling superparticles into small clusters selects the wavelength of the lasing modes, demonstrating an example of collective photonic behavior using these artificial solids.

INTRODUCTION

Throughout history, the emergence of complex patterns from the organization of smaller components has captivated humankind. This interest stems from the search for the mechanism driving the assembly process: Through multiple forces,^{1, 2} self-assembly leads to the formation of hierarchical superstructures.^{3, 4} Frequently, these superstructures perform a higher, collective function than their constituent building blocks.^{5, 6} Gaining control over self-assembly, therefore, represents a successful strategy to build materials with new properties.

Over the last three decades, scientists have learned to control the crystallization of atoms into nanoscale structures known as nanocrystals (NCs).⁷ Depending on their morphology, dimension, and chemical composition, NCs can manipulate electromagnetic radiation over a broad spectral range. Upon assembly into 3D mesoscale superstructures,^{2, 8-11} the properties of NCs hybridize through excitonic,¹²⁻¹⁴ electronic,¹⁵⁻¹⁸ magnetic,¹⁹⁻²¹ plasmonic,²²⁻²⁴ phononic,^{25, 26} and photonic^{6, 27, 28} coupling mechanisms. While the coupling strength is generally controlled by the distance between NCs,²⁹ the morphology of the superstructure plays an important role in mediating the interaction with external stimuli.

In the case of optical stimuli, Maxwell's equations predict the confinement of intense electromagnetic fields within a dielectric structure of dimensions comparable to the wavelength,³⁰ increasing the probability of absorption and scattering of light.^{6,31} Additionally, when the structure possesses rotational symmetry, light can become trapped at the surface through whispering gallery modes,^{28, 32, 33} resulting in a 3D resonator. Since these processes crucially depend on the morphology and refractive index of the structure,³⁴ there is a strong motivation to fabricate optical structures with well-defined size, shape, and composition.

Top-down microfabrication processes have succeeded in producing mesostructures with increasingly complex morphologies and high optical quality³⁵ to optimize and exploit the trapping of light for various applications. For instance, microfabricated ring resonators are regularly used as lasers²⁷ and second-harmonic generators,³⁶ as well as environmental^{37, 38} and mechanical³⁹ sensors. However, the fabrication of these optical structures relies on slow, complex, and expensive processes. Moreover, after fabrication these structures are usually bound to a substrate, limiting their deployment for *in situ* sensing. For these reasons, there are significant opportunities to develop more direct and cheaper experimental procedures to fabricate new classes of portable resonators by exploiting a recently developed, versatile,^{40, 41} scalable,⁴² and inexpensive technique known as emulsion-templated assembly.⁴³

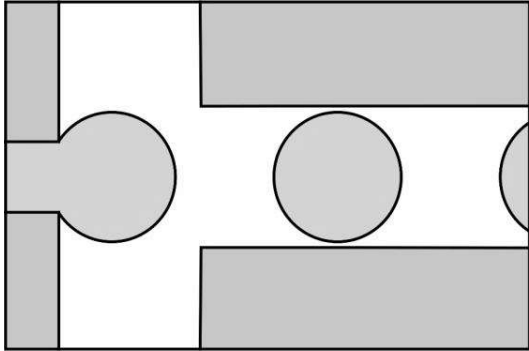
The simple act of shaking a mixture of oil and water in the presence of a surfactant can generate a polydisperse emulsion. Drying emulsion droplets that contain a dispersion of NCs leads to the formation of dense NC superstructures.^{40, 41, 44-47} These superstructures, known in the literature as superparticles,⁴⁸ supraparticles,⁴⁹ or supercrystals,⁴⁴ generally assume a spherical shape imposed by surface tension, although specific processing conditions can yield more complex morphologies, like cubic^{50, 51} and toroidal⁴³ shapes. These NC superparticles interact strongly with light through

Mie⁶ and whispering gallery modes,²⁸ and promise the introduction of more efficient, cheaper, and portable micro lasers,³⁴ upconversion media,⁵² and stimuli-responsive dielectric metasurfaces⁵³ for structural color applications.⁵⁴⁻⁵⁶ However, since the optical properties of the superparticles strongly depend on their dimensions, all applicative efforts are currently encumbered by the need for a reliable and general method to produce monodisperse NC superparticles.

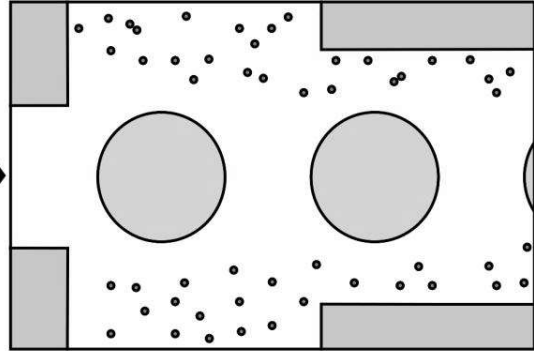
A monodisperse emulsion is a good starting point to fabricate monodisperse superparticles. Recently, droplet microfluidics has emerged as the technique of choice to generate emulsions with a polydispersity lower than 5%.⁵⁷⁻⁵⁹ Yet, the generated emulsions are sensitive to shear forces, and the mixing usually required to densify the droplets into superparticles results in significant size defocusing, as shown in Figure S1, thus jeopardizing the benefits of the microfluidic approach. Polymerizing the surface of the droplets can improve their stability by minimizing mass transport across the liquid/liquid interface.^{58, 60, 61} However, this strategy inherently impedes densification and is therefore unsuitable to form dense NC superparticles. Fluorosurfactants have shown excellent results in stabilizing water⁶²⁻⁶⁵ or oil⁴¹ droplets in fluorinated oil; yet, the use of fluorochemicals is environmentally unsustainable due to their resilience against degradation.⁶⁶

Here, we propose a general method to fabricate monodisperse, dense NC superparticles using a source-sink emulsion system. A schematic of this process is shown in Figure 1, and photos of the experimental setup are shown in Figure S2. We use droplet microfluidics to generate a monodisperse toluene-in-water “source” emulsion containing a dispersion of NCs, step 1. Then, we introduce a secondary “sink” emulsion consisting of much smaller droplets of an oil insoluble in water, such as hexadecane, step 2. The high internal pressure associated with the smaller emulsion drives the unidirectional mass transport of toluene from the source to the sink emulsion, progressively shrinking the toluene droplets and swelling the hexadecane droplets, step 3. Within

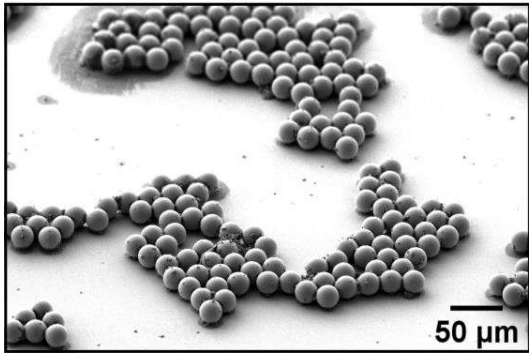
Step 1: Monodisperse "source" toluene emulsion containing nanocrystals



Step 2: Addition of "sink" hexadecane emulsion



Step 4: Monodisperse nanocrystal superparticles



Step 3: In-line source-to-sink mass transport of toluene

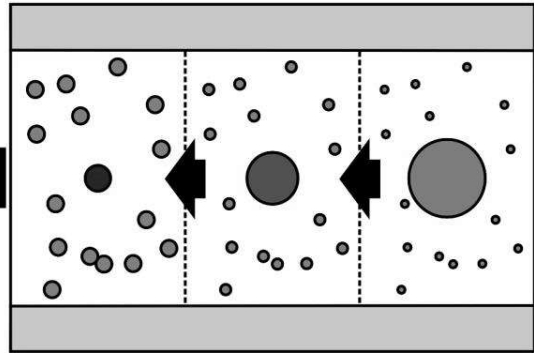


Figure 1: Schematic of the fabrication of monodisperse NC superparticles. **Step 1:** Generation of a monodisperse toluene-in-water “source” emulsion using droplet microfluidics. Each droplet contains a dispersion of NCs with initial volume fraction ϕ_i . **Step 2:** Introduction of a secondary hexadecane-in-water “sink” emulsion. The hexadecane droplets are three orders of magnitude smaller than the toluene droplets. **Step 3:** The sink emulsion swells with toluene from the source emulsion, shrinking the source droplets and ultimately forming NC superparticles. **Step 4:** After washing away the swollen sink emulsion, the NC superparticles appear monodisperse and spherical.

minutes, this process yields NC superparticles with a polydispersity as low as 2%, step 4. This approach can be immediately extended to a wide range of hydrophobic NCs to produce monodisperse, dense NC superparticles with core-only or core/shell morphologies and with sizes tunable by varying the initial NC volume fraction within the source droplets. The NC superparticles function as optical resonators, featuring lasing modes modulated by their spontaneous assembly into colloidal clusters.⁶⁷⁻⁷⁰ The proposed method represents a timely

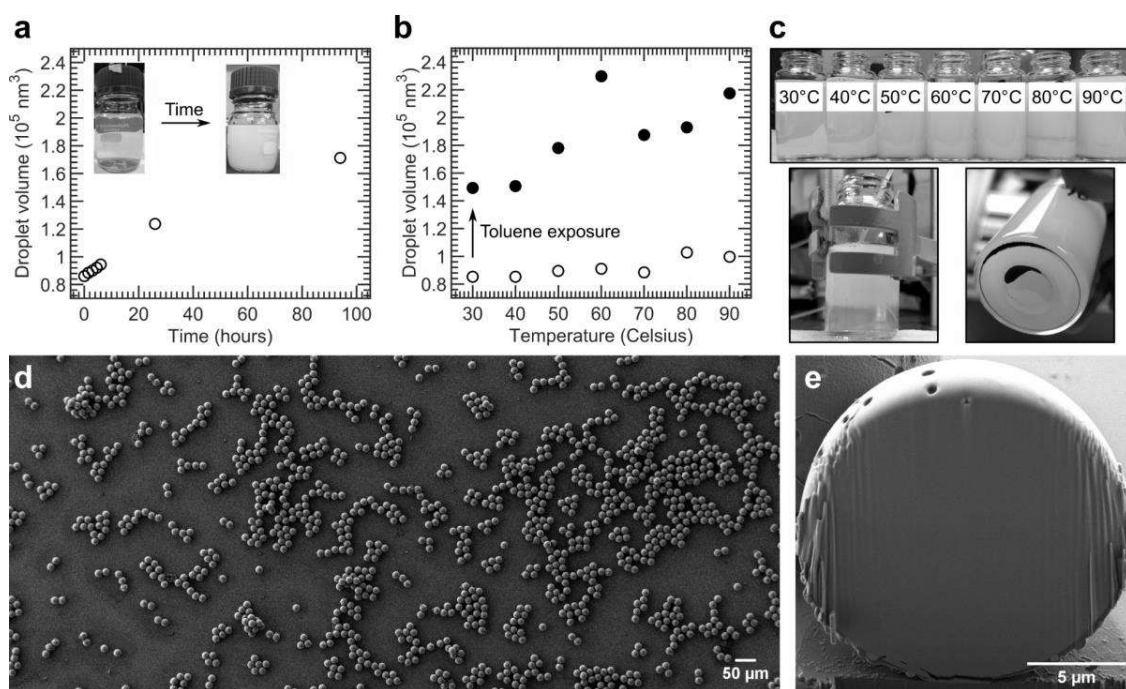


Figure 2: Exposure to a sink emulsion drives the formation of monodisperse NC superparticles. (a) Evolution of the “sink” hexadecane emulsion at room temperature when not exposed to toluene. The droplet volume is calculated from the average hydrodynamic radius extracted through dynamic light scattering. The photographs in the inset highlight the increase in turbidity of the hexadecane emulsion with time. (b) Evolution of the “sink” hexadecane emulsion as a function of temperature immediately prior to (open symbols) and after (closed symbols) exposure to the “source” toluene emulsion. The exposure time is 4 minutes. (c) (Top) Photographs of the collection vials showing the hexadecane emulsion after exposure to the toluene emulsion at different temperatures. The increase in turbidity with temperature correlates with the results of panel (b). (Bottom-left) Photograph of the 70 °C vial during sample collection. The difference in turbidity between the bottom and the top of the vial is due to the increased buoyancy of the hexadecane emulsion after exposure to toluene. (Bottom-right) The NC superparticles sediment within a few minutes after sample collection. (d) SEM micrograph of the NC superparticles deposited on a silicon substrate. (e) Cross-sectional SEM micrograph of a single NC superparticle prepared by FIB milling.

convergence of self-assembly over several length scales, paving the way to a more widespread use of NC superparticles as functional building blocks.

RESULTS AND DISCUSSION

We use a microfluidic cross junction as a generator for 140 μm monodisperse toluene droplets loaded with 5.7 nm spherical CdSe NCs at an initial volume fraction ϕ_i ; see Figure S3 for NC characterization, and the Materials and Methods section for details on droplet generation. These droplets represent the source emulsion and are stabilized by sodium dodecyl sulfate (SDS), a common surfactant for oil-in-water emulsions. Downstream from the droplet generator, we use another cross junction to introduce an emulsion of hexadecane in water, 1% hexadecane by weight, representing the sink emulsion. The sink emulsion, 55 nm \pm 38% in hydrodynamic diameter as measured by dynamic light scattering, is generated separately by extended ultra-sonication to reach an overall transparent appearance accompanied by a faint blue hue. A photograph of the sink emulsion is shown in the inset in Figure 2a. When left undisturbed at room temperature, the sink emulsion is remarkably stable with each droplet eventually doubling in volume, from 0.86 to $1.71 \times 10^5 \text{ nm}^3$, in 4 days due to Ostwald ripening;⁷¹ see Figure 2a. This microscopic change is accompanied by a macroscopic increase in turbidity, as demonstrated by the photograph in the inset. In contrast, exposing the sink emulsion to the NC-loaded source emulsion for only 4 minutes results in a comparable increase in the volume of the sink emulsion from 0.85 to $1.49 \times 10^5 \text{ nm}^3$, as shown in Figure 2b. This increase in volume of the sink emulsion is temperature-sensitive, with higher temperatures yielding a larger increase up to $2.14 \times 10^5 \text{ nm}^3$ at 90 °C. After exposure to the source emulsion, the sink emulsion shows a significant increase in turbidity, shown in Figure 2c. Visually inspecting the bottom of the collection vial reveals a dark sediment. Imaging the sediment with a scanning electron microscope (SEM) reveals an ensemble of monodisperse, spherical NC superparticles that have formed in 4 minutes; see Figure 2d. Milling a single superparticle using a focused ion beam (FIB) shows that the superparticles are densely packed with CdSe NCs, with no discernible voids, as shown in Figure 2e.

This proceeds by the sink emulsion swelling progressively by depleting toluene from the source emulsion. The relatively high aqueous solubility of toluene, 5.8×10^{-3} M,⁷² enables this mass transfer, while the much lower solubility of hexadecane, 2.6×10^{-11} M,⁷³ prohibits the reverse process. We confirm the generality of the source-sink emulsion approach by replacing hexadecane for another solvent also characterized by a lower aqueous solubility than toluene, such as dodecane, resulting in the formation of NC superparticles. Instead, replacing toluene for a solvent with a lower aqueous solubility, such as hexane, 1.6×10^{-4} M,⁷⁴ inhibits mass transport and does not lead to monodisperse NC superparticles within the investigated residence times. Increasing either the residence time, the concentration of the sink emulsion, or the initial NC volume fraction may expand the use of source-sink emulsion approach to solvents with a lower aqueous solubility than toluene.

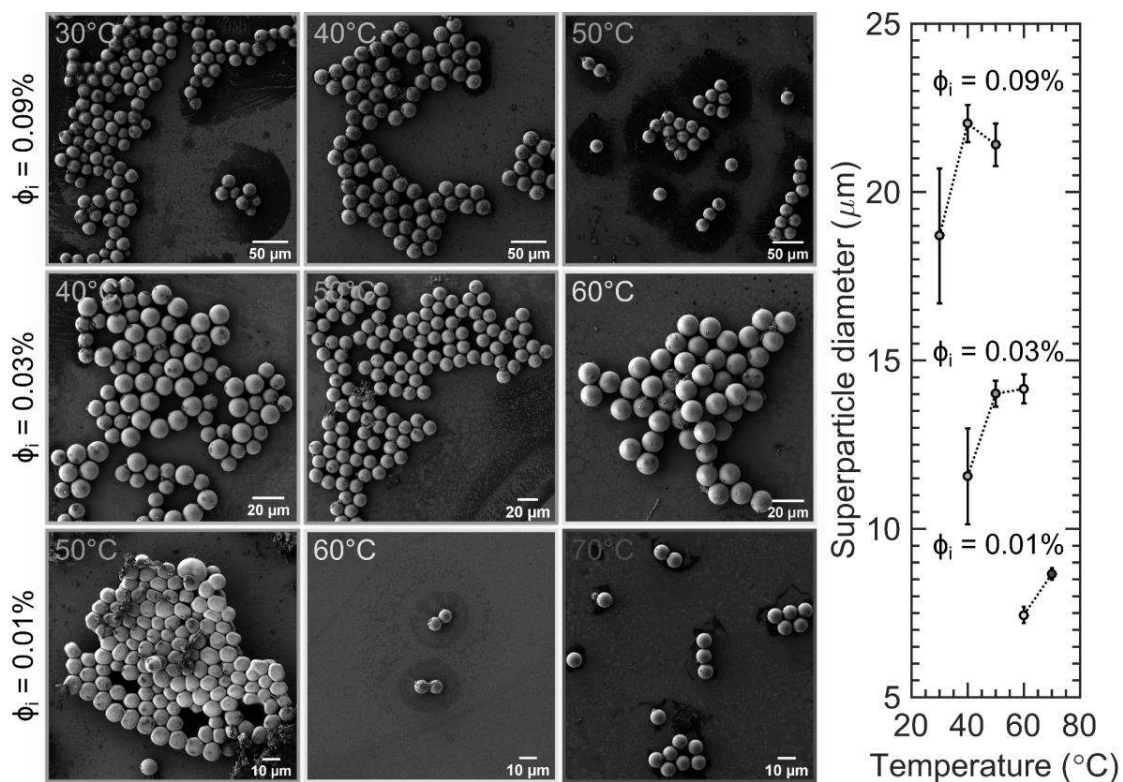


Figure 3: Fabrication of NC superparticles of different sizes and morphologies. (Bottom to top) Increasing the initial NC volume fraction, ϕ_i , results in overall larger superparticles. (Left to right) Increasing the temperature of the aqueous phase results in overall more monodisperse and spherical superparticles. These changes have been quantified in the graph, indicating the average superparticle size (symbol) and standard deviation (error bars).

The initial NC volume fraction within the toluene droplets, ϕ_i , determines the average size of the resulting superparticles, as shown in Figure 3. Varying ϕ_i from 0.01% to 0.09% increases the average diameter of the spherical superparticles, indicated by the symbols, from 7 to 23 μm . Using even higher ϕ_i leads to larger superparticles which sediment in the residency channel before reaching the collection vial. Instead, using lower ϕ_i leads to smaller superparticles that are still buoyant upon reaching the collection vial, creaming to the air/liquid interface. An example of this is shown in the bottom-left panel of Figure 3, where the toluene droplets have reached the air/liquid interface while still buoyant, assembling to form a monolayer. The droplets have then deformed

to maximize surface coverage of the interface,^{41, 75} creating a tiling pattern of anisotropic superparticles.

Adjusting the temperature of the aqueous phase during the co-residency time of source and sink emulsions affects the formation of the superparticles, as shown in Figure 3. Specifically, increasing the temperature results in an increase in the average diameter of the superparticles while concurrently decreasing their polydispersity, indicated by the error bars. This is most likely due to the temperature-driven increase in solubility and diffusion rate of toluene in the aqueous phase,⁷² which decreases the residency time required to form the NC superparticles. In turn, this also decreases the probability of size defocusing,⁷¹ since the time required by the droplets to form superparticles decreases with increasing temperature, minimizing the possibility of droplet collision and merging; see Supplementary note S1 for additional discussion. When using a sufficiently high temperature for a given value of ϕ_i , for instance, 50 °C for $\phi_i = 0.09\%$, this method yields NC superparticles with a polydispersity as low as 2%.

The source-sink emulsion method can be readily generalized to other NC systems. We synthesize 12.2 nm anisotropic core/shell CdSe/CdS NCs with unity photoluminescence (PL) quantum yield by following a recent report;⁷⁶ see Figure S4 for NC characterization. Also in this case, the source-sink emulsion method yields spherical superparticles, as shown in Figure 4a. The 9.0 μm

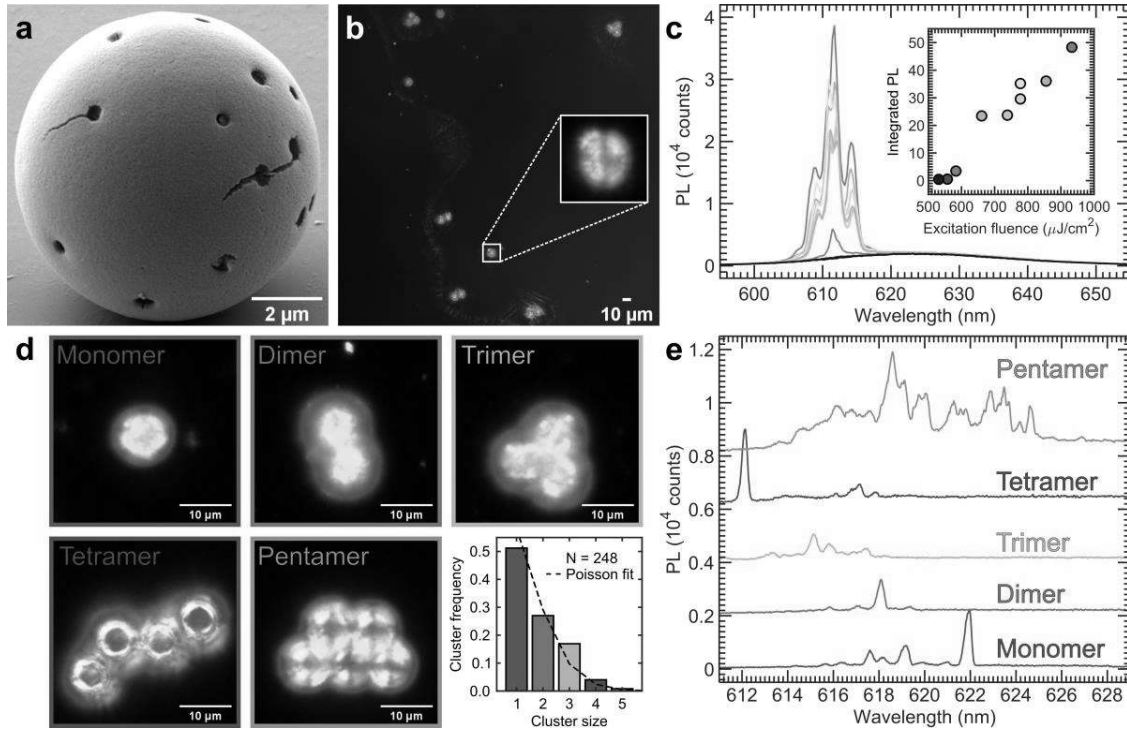


Figure 4: Lasing from NC superparticles produced through the source-sink emulsion approach. (a) SEM micrograph of a spherical superparticle of anisotropic CdSe/CdS NCs with unity PL quantum yield. (b) Dark-field optical micrograph of the monodisperse superparticles. (c) PL spectrum of a superparticle excited at 500 nm as a function of the excitation fluence. The inset shows the integrated intensity of the lasing peaks as a function of excitation fluence. (d) Dark-field optical micrographs of various clusters of NC superparticles and a histogram describing their occurrence from a sample of $N = 248$ clusters. A fit to a zero-truncated Poisson distribution is shown by a dashed line. (e) PL spectra of the superparticle clusters shown in (d) when exciting above lasing threshold. The spectra have been progressively shifted for clarity.

superparticles appear monodisperse, as illustrated by the dark-field micrograph in Figure 4b. Upon excitation with 500 nm light, the superparticles show a photoluminescence (PL) spectrum centered around 625 nm; see Figure 4c. When increasing the excitation fluence above a threshold of 550 $\mu\text{J}/\text{cm}^2$, we observe the emergence of sharp peaks in PL that we attribute to lasing, as demonstrated by the super-linear increase in the integrated PL intensity with fluence shown in inset. Exciting with wavelengths below 500 nm results in the increase of lasing threshold, likely because of heating losses due to absorption of light by the thick CdS shell.²⁸

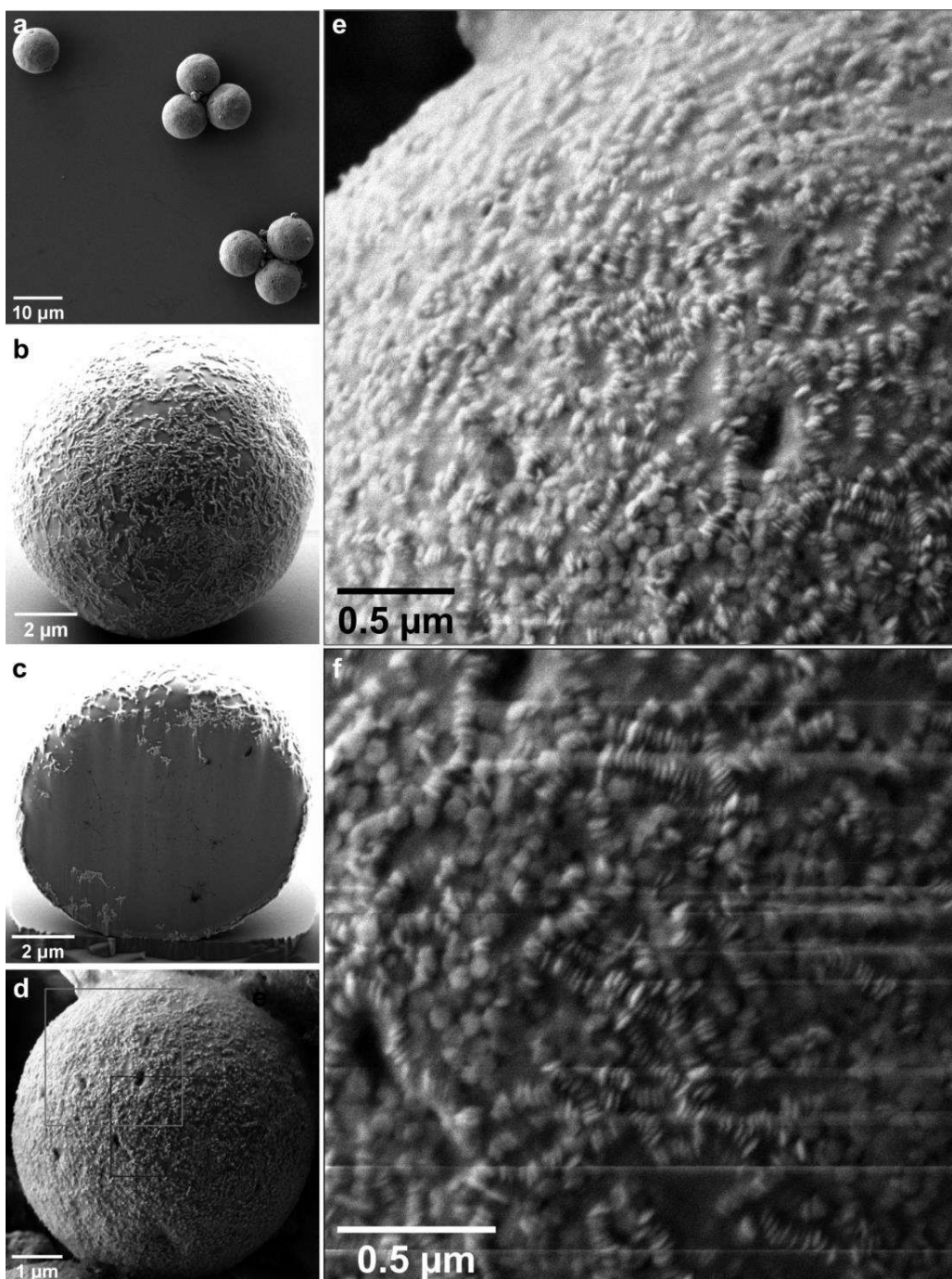


Figure 5: Core/shell NC superparticles. SEM micrographs of (a,b) monodisperse core/shell NC superparticles from spherical PbS/CdS and discoidal NaGdF₄ NCs, and (c) their cross-sections prepared by FIB milling, revealing that the spherical NCs mostly reside in the core of the superparticles while the disks are located in the shell. (d-f) SEM micrographs of the surface of the superparticles show that the disks tend to stack rather than to tile at the surface of the superparticles. Streaking features are due to charging.

A closer inspection of the micrograph in Figure 4b reveals that the superparticles spontaneously

assemble into small clusters,^{67, 68} or colloidal molecules,^{69, 70} upon drop-casting. Figure 4d shows dark-field images of a monomer, a dimer, a trimer, a tetramer, and a pentamer that we are able to locate on the silicon substrate. The frequency with which these clusters occur decreases quickly with cluster size by following a zero-truncated Poisson distribution, as shown by the histogram in Figure 4d. When exciting above lasing threshold, each of these clusters lases at different wavelengths, as shown in Figure 4e. Lasing of an isolated superparticle occurs via the confinement of light emitted by NCs to the surface of the superparticle through whispering gallery modes.²⁸ We argue that the assembly of superparticles into clusters likely leads to the hybridization of the whispering gallery modes of a single superparticle,⁷⁷ determining the wavelength of the lasing modes of a superparticle cluster. The quality factor of the superparticles, measured as $Q = \lambda/\Delta\lambda = 1600 \pm 18\%$, does not depend on the morphology of the cluster and is comparable to that of micro-fabricated ring resonators of equal diameter,²⁷ corresponding to an average lifetime of the energy stored in the resonator of $\tau = Q\lambda/c = 3.3$ ps, where λ is the resonant wavelength, $\Delta\lambda$ the full-width at half-maximum of the resonance, and c the speed of light.

The source-sink emulsion approach can also be used to fabricate more complex superparticle architectures, as shown in Figure 5. Loading the microfluidic toluene droplets with a mixture of NCs with different shapes readily results in monodisperse core/shell NC superparticles; see Figure 5a. To achieve this morphology, we purposefully targeted a combination of NC shapes, disks and spheres,^{78, 79} that hinder the formation of binary phases, therefore triggering the spontaneous phase separation of NCs during the assembly process, see Figure S5-S6 for NC characterization. Using a total volume fraction of spheres four times larger than that of disks results in superparticles with a dense core occupied by PbS/CdS spheres, 4.3 nm in diameter, and a thin shell formed by NaGdF₄ disks, 57 nm in diameter and 17 nm in thickness, as shown in Figure 5b-c. While the PbS/CdS

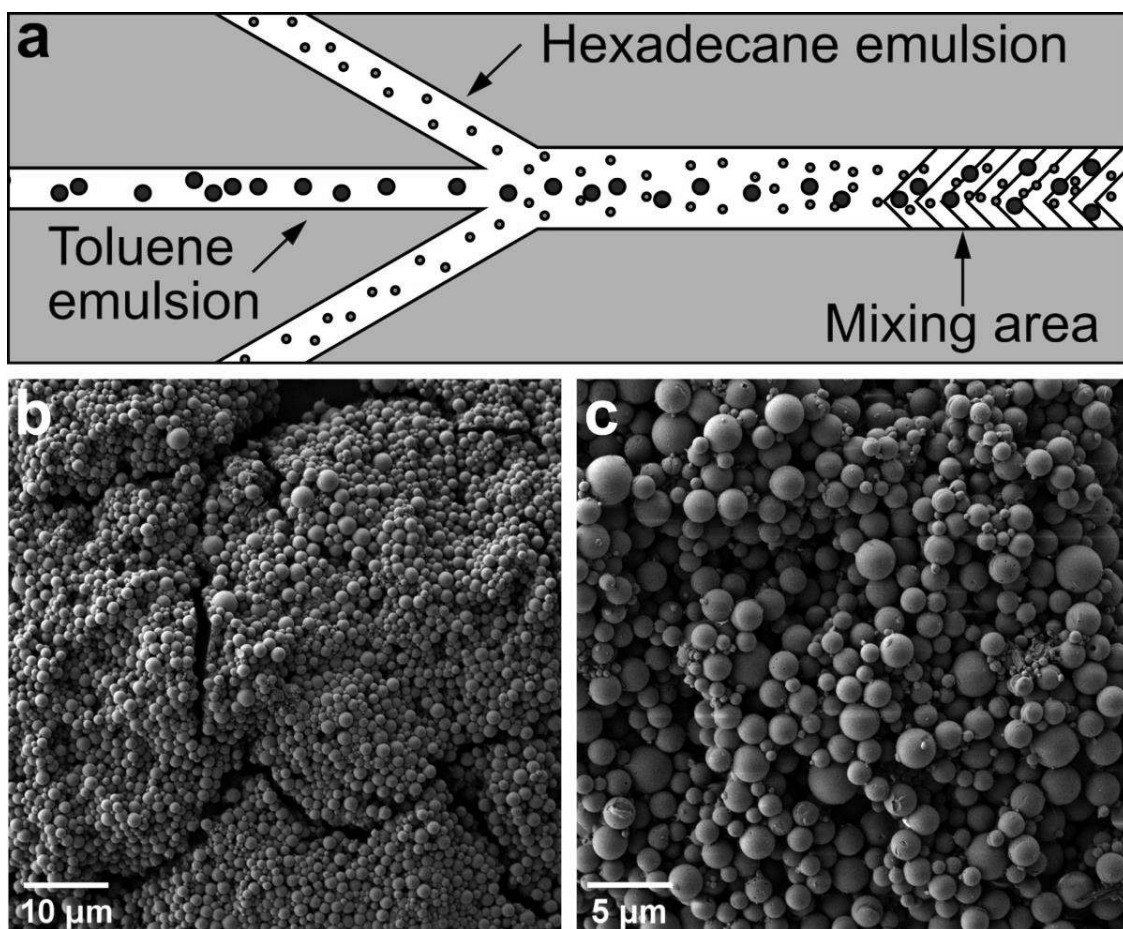


Figure 6: In-line production of NC superparticles without the use of droplet microfluidics. (a) A herringbone mixer can be used to facilitate mass transport between the toluene and hexadecane emulsions. (b-c) By starting with a toluene shake-emulsion, large amounts of polydisperse NC superparticles can be readily produced.

spheres are too small to be distinguished in SEM, the NaGdF₄ disks are well within the resolution of the microscope and show a tendency to stack rather than to tile the surface of the superparticles, confirming a disk-to-disk affinity stronger than disk-to-sphere;^{78, 79} see Figure 5d-f. FIB milling a single superparticle highlights the shape-driven phase separation of NCs, although a few disks are still present below the surface of the superparticle. Due to their higher volume fraction, the smaller spherical NCs likely reach the nucleation threshold first,^{40, 44, 80} achieving phase separation by segregating the disks to the outer volume of the droplet at the later stages of assembly. Therefore,

the observation of a core/shell morphology represents indirect evidence for the homogeneous nucleation of NCs under spherical confinement.

CONCLUSIONS

We demonstrate a general, rapid approach to consistently drive the formation of monodisperse NC superparticles. This approach relies on the interplay of two oil-in-water emulsions: a “source” emulsion of toluene loaded with NCs and a “sink” emulsion of an oil insoluble in water, like hexadecane. Mixing the two emulsions results in the temperature-controlled mass transport of toluene from the source to the sink emulsion, leading to the formation of spherical NC superparticles within minutes. Using monodisperse toluene droplets generated through droplet microfluidics results in monodisperse NC superparticles, independent of NC size, shape, composition, or polydispersity. However, the use of droplet microfluidics is not necessary for the source-sink emulsion approach to work. Exposing the sink emulsion to a polydisperse source emulsion prepared by vortex-mixing results in the generation of polydisperse NC superparticles, as shown in Figure 6. Importantly, the source-sink emulsion approach provides the crucial benefit of accelerating the removal of the toluene from the source emulsion, achieving in minutes what would otherwise require several hours via evaporation.^{40, 44, 80}

We validate the versatility of the source-sink emulsion approach by leveraging recent advances in NC synthesis. Using NCs with unity PL quantum yield leads to clusters of monodisperse superparticles that feature morphology-dependent lasing modes with an average quality factor of 1600. Instead, mixing two incompatible NC shapes yields monodisperse superparticles with a complex morphology characterized by the shape-driven phase separation of NCs in the core and

the shell of the superparticle. Tailoring the morphology and size of the ligand corona may offer an additional steric knob to influence the final structure of the superparticles.^{81, 82} The source-sink emulsion approach leads to the formation of functional NC superparticles of various sizes, shapes, and morphologies in just a few minutes, paving the way to a more extended use of these complex artificial solids towards applications in photonics,^{6, 52} magnetotherapy,²¹ energy storage,⁸³ and catalysis.⁸⁴

MATERIALS AND METHODS

NC synthesis. Detailed synthetic procedures are provided in the supporting information. CdSe,^{44, 85} CdSe/CdS,⁷⁶ PbS,⁸⁶ PbS/CdS⁸⁷ are synthesized according to literature reports and dispersed in toluene after purification. NaGdF₄ NCs are synthesized by following a procedure described in the supporting information. The NC concentration for CdSe⁸⁸ and PbS⁸⁹ NCs is determined from spectrophotometry by following reported sizing curves. The concentration for the other NCs is determined by drying and weighing the pellet.

Preparation of the sink emulsion: 90 g of 200 mM SDS in Milli-Q water are added to a 100 mL media bottle (Fisher). 10 g of an oil insoluble in water, such as hexadecane or dodecane, are subsequently added. The media bottle is capped, and the contents are mixed by continuous inversion for a few seconds. The bottle is then sonicated for 90 minutes by using a bath sonicator (Branson 1510). The bottle is then removed from the sonicator, and the contents are mixed by continuous inversion for a few seconds. At this point, the emulsion appears milky, corresponding to an average hydrodynamic diameter for the droplets of 137 nm \pm 35%, as determined by dynamic light scattering (Malvern Zetasizer). The bottle is then uncapped and placed in an ice bath. After

placing the tip of the ultrasonicator (Misonix Sonicator 3000) in the emulsion, the contents of the media bottle are sonicated for 120 minutes (peak power 84 W, 50% duty cycle). Afterwards, the emulsion has a mostly clear appearance with a faint blue hue, corresponding to an average hydrodynamic diameter of $55 \text{ nm} \pm 37\%$ as measured by DLS. The emulsion is then immediately diluted ten-fold with Milli-Q water to reach an oil concentration of 1% w/w in an aqueous solution of 20 mM SDS. The sink emulsion is used immediately or placed in the fridge and used within 24 hours.

Microfluidic droplet generation. We generate monodisperse toluene droplets by using a commercial droplet generator glass chip (Darwin microfluidics, T-26) connected to a multi-channel pressure regulator (Elveflow, OB1 MK3+). The dispersed phase of the emulsion consists in a dispersion of NCs with a known volume fraction in toluene, filtered before use with a $0.22 \text{ }\mu\text{m}$ PVDF or PTFE syringe filter. The continuous phase of the emulsion consists in a 20 mM solution of SDS in Milli-Q water filtered before use with a $0.22 \text{ }\mu\text{m}$ PVDF syringe filter. The sink emulsion phase is prepared as described above and consists in a 1% w/w of hexadecane or dodecane in 20 mM SDS in Milli-Q water. The microfluidic chip is operated at pressures of 1 bar/1 bar/2 bar for dispersed/continuous/sink emulsion channels. Increasing the overall pressure while maintaining the same ratios results in smaller toluene droplets. Instead, the herringbone mixer chip is operated at 1 bar/1 bar pressures for source/sink emulsion phases. In all cases, the outlet of the chip is connected to a PFA tubing (ID 0.5 mm, OD 1.6 mm, Cole Parmer). The tubing has an overall length of 11.5 m and is wrapped around a cylindrical copper rod (OD 38 mm, length 0.33 m, McMaster Carr) engraved with a spiral of 0.8 mm radius and 3.2 mm pitch to improve thermal contact.⁹⁰ The temperature of the rod is controlled by means of a temperature controller (J-KEM) by embedding a heating cartridge (Briskheat) and a thermocouple (J-KEM) within the rod. The

samples are collected in 20 mL scintillation vials filled with 5 mL of the sink emulsion. After collection, the vials are left uncapped and undisturbed on a hot plate set at 50 °C for overnight. The samples are then washed three times by centrifuging at 100 g and replacing the supernatant with 20 mM SDS in Milli-Q water, and eventually concentrated to 1 mL.

Electron microscopy. The samples are prepared for SEM imaging by drop casting 40 μ L of the superparticle dispersion on a clean piece of silicon wafer, followed by vacuum drying. The wafer is then dipped twice in a cleaning solution of water and isopropanol, 1:2 by volume, to remove the excess surfactant without redispersing the superparticles, followed by vacuum drying. The samples are imaged using a Tescan S8252X operated at 2 kV and 100 pA. FIB milling of the superparticles is performed with an ion voltage and current of 30 kV and 100 nA, respectively.

Lasing experiments. 500 nm light from an optical parametric amplifier (Coherent OperaHP) pumped by an ultrafast laser (Coherent Monaco 1035, 0.272 ps pulsewidth) is coupled to a multimode optical fiber. The output of the fiber is collimated and directed through a 50x/NA 0.8 objective (Olympus MPlanFL N). The full-width at half-maximum of the spot size in the sample plane is 14.0 μ m. Light emitted by the superparticles is collected through the same objective and focused to an optical fiber coupled to a spectrometer (Horiba iHR550 monochromator and Symphony II CCD). The excitation beam is filtered from the signal via appropriate long-pass filters placed before the collection fiber.

ASSOCIATED CONTENT

Supporting Information.

The following files are available free of charge.

Detailed description of the microfluidic chips and setups used, NC synthesis, micrographs of the NCs, optical characterization of the NCs (PDF)

AUTHOR INFORMATION

Corresponding Author

*cbmurray@sas.upenn.edu

Author Contributions

E.M. and T.E.K. conceived the project. E.M. and W.L. synthesized the NCs. E.M. and S.v.D. designed the assembly process and performed experiments. E.M. and A.W.K. performed the electron microscopy studies. E.M. and S.J.N. performed the lasing experiments. T.E.K. and C.B.M. supervised the project. E.M. wrote the initial draft. The results were discussed with all authors. The manuscript was written through contributions of all authors. All authors have given approval to the final version of the manuscript.

Notes

The authors declare no competing financial interest(s). Aspects of this work have been included in a provisional U.S. patent filing.

ACKNOWLEDGMENT

The authors acknowledge primary support from the Office of Naval Research Multidisciplinary University Research Initiative Award ONR N00014-18-1-2497. The authors also acknowledge secondary support from the Semiconductor Research Corporation (SRC) under the

Nanomanufacturing Materials and Processes (NMP) trust via Task 2797.001 for part of the SEM imaging, and the National Science Foundation (NSF) through the University of Pennsylvania Materials Research Science and Engineering Center (MRSEC) under Award No. DMR1720530 for the lasing experiments. C.B.M. acknowledges the Richard Perry University Professorship at the University of Pennsylvania.

REFERENCES

1. Bishop, K. J. M.; Wilmer, C. E.; Soh, S.; Grzybowski, B. A., Nanoscale Forces and Their Uses in Self-Assembly. *Small* **2009**, *5* (14), 1600-1630.
2. Marino, E.; Vasilyev, O. A.; Klufft, B. B.; Stroink, M. J. B.; Kondrat, S.; Schall, P., Controlled deposition of nanoparticles with critical Casimir forces. *Nanoscale Horizons* **2021**, *6* (9), 751-758.
3. Whitesides George, M.; Grzybowski, B., Self-Assembly at All Scales. *Science* **2002**, *295* (5564), 2418-2421.
4. Marino, E.; Balazs, D. M.; Crisp, R. W.; Hermida-Merino, D.; Loi, M. A.; Kodger, T. E.; Schall, P., Controlling Superstructure–Property Relationships via Critical Casimir Assembly of Quantum Dots. *The Journal of Physical Chemistry C* **2019**, *123* (22), 13451-13457.
5. Teyssier, J.; Saenko, S. V.; van der Marel, D.; Milinkovitch, M. C., Photonic crystals cause active colour change in chameleons. *Nature Communications* **2015**, *6* (1), 6368.
6. Marino, E.; Sciortino, A.; Berkhout, A.; MacArthur, K. E.; Heggen, M.; Gregorkiewicz, T.; Kodger, T. E.; Capretti, A.; Murray, C. B.; Koenderink, A. F.; Messina, F.; Schall, P., Simultaneous Photonic and Excitonic Coupling in Spherical Quantum Dot Supercrystals. *ACS Nano* **2020**, *14* (10), 13806-13815.
7. Murray, C. B.; Norris, D. J.; Bawendi, M. G., Synthesis and characterization of nearly monodisperse CdE (E = sulfur, selenium, tellurium) semiconductor nanocrystallites. *Journal of the American Chemical Society* **1993**, *115* (19), 8706-8715.
8. Murray, C. B.; Kagan, C. R.; Bawendi, M. G., Self-Organization of CdSe Nanocrystallites into Three-Dimensional Quantum Dot Superlattices. *Science* **1995**, *270* (5240), 1335-1338.
9. Wu, L.; Willis, J. J.; McKay, I. S.; Diroll, B. T.; Qin, J.; Cargnello, M.; Tassone, C. J., High-temperature crystallization of nanocrystals into three-dimensional superlattices. *Nature* **2017**, *548* (7666), 197-201.
10. Santos, P. J.; Gabrys, P. A.; Zornberg, L. Z.; Lee, M. S.; Macfarlane, R. J., Macroscopic materials assembled from nanoparticle superlattices. *Nature* **2021**, *591* (7851), 586-591.
11. Shevchenko, E. V.; Podsiadlo, P.; Wu, X.; Lee, B.; Rajh, T.; Morin, R.; Pelton, M., Visualizing Heterogeneity of Monodisperse CdSe Nanocrystals by Their Assembly into Three-Dimensional Supercrystals. *ACS Nano* **2020**, *14* (11), 14989-14998.
12. Schedelbeck, G.; Wegscheider, W.; Bichler, M.; Abstreiter, G., Coupled Quantum Dots Fabricated by Cleaved Edge Overgrowth: From Artificial Atoms to Molecules. *Science* **1997**, *278* (5344), 1792-1795.

13. Bayer, M.; Hawrylak, P.; Hinzer, K.; Fafard, S.; Korkusinski, M.; Wasilewski, Z. R.; Stern, O.; Forchel, A., Coupling and Entangling of Quantum States in Quantum Dot Molecules. *Science* **2001**, *291* (5503), 451-453.
14. Rowland, C. E.; Fedin, I.; Zhang, H.; Gray, S. K.; Govorov, A. O.; Talapin, D. V.; Schaller, R. D., Picosecond energy transfer and multiexciton transfer outpaces Auger recombination in binary CdSe nanoplatelet solids. *Nature Materials* **2015**, *14* (5), 484-489.
15. Lan, X.; Chen, M.; Hudson, M. H.; Kamysbayev, V.; Wang, Y.; Guyot-Sionnest, P.; Talapin, D. V., Quantum dot solids showing state-resolved band-like transport. *Nature Materials* **2020**, *19* (3), 323-329.
16. Choi, J.-H.; Fafarman, A. T.; Oh, S. J.; Ko, D.-K.; Kim, D. K.; Diroll, B. T.; Muramoto, S.; Gillen, J. G.; Murray, C. B.; Kagan, C. R., Bandlike Transport in Strongly Coupled and Doped Quantum Dot Solids: A Route to High-Performance Thin-Film Electronics. *Nano Letters* **2012**, *12* (5), 2631-2638.
17. Talgorn, E.; Gao, Y.; Aerts, M.; Kunneman, L. T.; Schins, J. M.; Savenije, T. J.; van Huis, M. A.; van der Zant, H. S. J.; Houtepen, A. J.; Siebbeles, L. D. A., Unity quantum yield of photogenerated charges and band-like transport in quantum-dot solids. *Nature Nanotechnology* **2011**, *6* (11), 733-739.
18. Lee, J.-S.; Kovalenko, M. V.; Huang, J.; Chung, D. S.; Talapin, D. V., Band-like transport, high electron mobility and high photoconductivity in all-inorganic nanocrystal arrays. *Nature Nanotechnology* **2011**, *6* (6), 348-352.
19. Chen, J.; Dong, A.; Cai, J.; Ye, X.; Kang, Y.; Kikkawa, J. M.; Murray, C. B., Collective Dipolar Interactions in Self-Assembled Magnetic Binary Nanocrystal Superlattice Membranes. *Nano Letters* **2010**, *10* (12), 5103-5108.
20. Chen, J.; Ye, X.; Oh, S. J.; Kikkawa, J. M.; Kagan, C. R.; Murray, C. B., Bistable Magnetoresistance Switching in Exchange-Coupled CoFe₂O₄-Fe₃O₄ Binary Nanocrystal Superlattices by Self-Assembly and Thermal Annealing. *ACS Nano* **2013**, *7* (2), 1478-1486.
21. Yang, Y.; Wang, B.; Shen, X.; Yao, L.; Wang, L.; Chen, X.; Xie, S.; Li, T.; Hu, J.; Yang, D.; Dong, A., Scalable Assembly of Crystalline Binary Nanocrystal Superparticles and Their Enhanced Magnetic and Electrochemical Properties. *Journal of the American Chemical Society* **2018**, *140* (44), 15038-15047.
22. Mueller, N. S.; Okamura, Y.; Vieira, B. G. M.; Juergensen, S.; Lange, H.; Barros, E. B.; Schulz, F.; Reich, S., Deep strong light-matter coupling in plasmonic nanoparticle crystals. *Nature* **2020**, *583* (7818), 780-784.
23. Guo, J.; Kim, J.-Y.; Yang, S.; Xu, J.; Choi, Y. C.; Stein, A.; Murray, C. B.; Kotov, N. A.; Kagan, C. R., Broadband Circular Polarizers via Coupling in 3D Plasmonic Meta-Atom Arrays. *ACS Photonics* **2021**, *8* (5), 1286-1292.
24. Ye, X.; Chen, J.; Diroll, B. T.; Murray, C. B., Tunable Plasmonic Coupling in Self-Assembled Binary Nanocrystal Superlattices Studied by Correlated Optical Microspectrophotometry and Electron Microscopy. *Nano Letters* **2013**, *13* (3), 1291-1297.
25. Poyser, C. L.; Czerniuk, T.; Akimov, A.; Diroll, B. T.; Gaulding, E. A.; Salasyuk, A. S.; Kent, A. J.; Yakovlev, D. R.; Bayer, M.; Murray, C. B., Coherent Acoustic Phonons in Colloidal Semiconductor Nanocrystal Superlattices. *ACS Nano* **2016**, *10* (1), 1163-1169.
26. Bozyigit, D.; Yazdani, N.; Yarema, M.; Yarema, O.; Lin, W. M. M.; Volk, S.; Vuttivorakulchai, K.; Luisier, M.; Juranyi, F.; Wood, V., Soft surfaces of nanomaterials enable strong phonon interactions. *Nature* **2016**, *531* (7596), 618-622.

27. le Feber, B.; Prins, F.; De Leo, E.; Rabouw, F. T.; Norris, D. J., Colloidal-Quantum-Dot Ring Lasers with Active Color Control. *Nano Letters* **2018**, *18* (2), 1028-1034.
28. Montanarella, F.; Urbonas, D.; Chadwick, L.; Moerman, P. G.; Baesjou, P. J.; Mahrt, R. F.; van Blaaderen, A.; Stöferle, T.; Vanmaekelbergh, D., Lasing Supraparticles Self-Assembled from Nanocrystals. *ACS Nano* **2018**, *12* (12), 12788-12794.
29. Kagan, C. R.; Murray, C. B., Charge transport in strongly coupled quantum dot solids. *Nature Nanotechnology* **2015**, *10* (12), 1013-1026.
30. Kuznetsov, A. I.; Miroshnichenko, A. E.; Brongersma, M. L.; Kivshar, Y. S.; Luk'yanchuk, B., Optically resonant dielectric nanostructures. *Science* **2016**, *354* (6314), aag2472, 846.
31. Bohren, C. F.; Huffman, D. R., Chapter 4: Absorption and Scattering by a Sphere. In *Absorption and Scattering of Light by Small Particles*, John Wiley & Sons: 1998; pp 82-129.
32. Jana, S.; Xu, X.; Klymchenko, A.; Reisch, A.; Pons, T., Microcavity-Enhanced Fluorescence Energy Transfer from Quantum Dot Excited Whispering Gallery Modes to Acceptor Dye Nanoparticles. *ACS Nano* **2021**, *15* (1), 1445-1453.
33. Du, W.; Zhang, S.; Wu, Z.; Shang, Q.; Mi, Y.; Chen, J.; Qin, C.; Qiu, X.; Zhang, Q.; Liu, X., Unveiling lasing mechanism in CsPbBr₃ microsphere cavities. *Nanoscale* **2019**, *11* (7), 3145-3153.
34. Chang, H.; Zhong, Y.; Dong, H.; Wang, Z.; Xie, W.; Pan, A.; Zhang, L., Ultrastable low-cost colloidal quantum dot microlasers of operative temperature up to 450 K. *Light: Science & Applications* **2021**, *10* (1), 60.
35. Armani, D. K.; Kippenberg, T. J.; Spillane, S. M.; Vahala, K. J., Ultra-high-Q toroid microcavity on a chip. *Nature* **2003**, *421* (6926), 925-928.
36. Linden, S.; Niesler, F. B. P.; Förstner, J.; Grynko, Y.; Meier, T.; Wegener, M., Collective Effects in Second-Harmonic Generation from Split-Ring-Resonator Arrays. *Physical Review Letters* **2012**, *109* (1), 015502.
37. Armani, A. M.; Kulkarni, R. P.; Fraser, S. E.; Flagan, R. C.; Vahala, K. J., Label-Free, Single-Molecule Detection with Optical Microcavities. *Science* **2007**, *317* (5839), 783-787.
38. Zhu, J.; Ozdemir, S. K.; Xiao, Y.-F.; Li, L.; He, L.; Chen, D.-R.; Yang, L., On-chip single nanoparticle detection and sizing by mode splitting in an ultrahigh-Q microresonator. *Nature Photonics* **2010**, *4* (1), 46-49.
39. Zhao, X.; Tsai, J. M.; Cai, H.; Ji, X. M.; Zhou, J.; Bao, M. H.; Huang, Y. P.; Kwong, D. L.; Liu, A. Q., A nano-opto-mechanical pressure sensor via ring resonator. *Opt. Express* **2012**, *20* (8), 8535-8542.
40. Marino, E.; Keller, A. W.; An, D.; van Dongen, S.; Kodger, T. E.; MacArthur, K. E.; Heggen, M.; Kagan, C. R.; Murray, C. B.; Schall, P., Favoring the Growth of High-Quality, Three-Dimensional Supercrystals of Nanocrystals. *The Journal of Physical Chemistry C* **2020**, *124* (20), 11256-11264.
41. Tang, Y.; Gomez, L.; Lesage, A.; Marino, E.; Kodger, T. E.; Meijer, J.-M.; Kolpakov, P.; Meng, J.; Zheng, K.; Gregorkiewicz, T.; Schall, P., Highly Stable Perovskite Supercrystals via Oil-in-Oil Templating. *Nano Letters* **2020**, *20* (8), 5997-6004.
42. Yadavali, S.; Jeong, H.-H.; Lee, D.; Issadore, D., Silicon and glass very large scale microfluidic droplet integration for terascale generation of polymer microparticles. *Nature Communications* **2018**, *9* (1), 1222.
43. Velev, O. D.; Lenhoff, A. M.; Kaler, E. W., A Class of Microstructured Particles Through Colloidal Crystallization. *Science* **2000**, *287* (5461), 2240-2243.

44. Marino, E.; Kodger, T. E.; Wegdam, G. H.; Schall, P., Revealing Driving Forces in Quantum Dot Supercrystal Assembly. *Advanced Materials* **2018**, *30* (43), 1803433.
45. de Nijs, B.; Dussi, S.; Smalenburg, F.; Meeldijk, J. D.; Groenendijk, D. J.; Fillion, L.; Imhof, A.; van Blaaderen, A.; Dijkstra, M., Entropy-driven formation of large icosahedral colloidal clusters by spherical confinement. *Nature Materials* **2015**, *14* (1), 56-60.
46. Lacava, J.; Born, P.; Kraus, T., Nanoparticle Clusters with Lennard-Jones Geometries. *Nano Letters* **2012**, *12* (6), 3279-3282.
47. Kister, T.; Mravlak, M.; Schilling, T.; Kraus, T., Pressure-controlled formation of crystalline, Janus, and core-shell supraparticles. *Nanoscale* **2016**, *8* (27), 13377-13384.
48. Wang, T.; LaMontagne, D.; Lynch, J.; Zhuang, J.; Cao, Y. C., Colloidal superparticles from nanoparticle assembly. *Chemical Society Reviews* **2013**, *42* (7), 2804-2823.
49. Wintzheimer, S.; Granath, T.; Oppmann, M.; Kister, T.; Thai, T.; Kraus, T.; Vogel, N.; Mandel, K., Supraparticles: Functionality from Uniform Structural Motifs. *ACS Nano* **2018**, *12* (6), 5093-5120.
50. Wang, T.; Wang, X.; LaMontagne, D.; Wang, Z.; Wang, Z.; Cao, Y. C., Shape-Controlled Synthesis of Colloidal Superparticles from Nanocubes. *Journal of the American Chemical Society* **2012**, *134* (44), 18225-18228.
51. Wang, D.; Hermes, M.; Kotni, R.; Wu, Y.; Tasios, N.; Liu, Y.; de Nijs, B.; van der Wee, E. B.; Murray, C. B.; Dijkstra, M.; van Blaaderen, A., Interplay between spherical confinement and particle shape on the self-assembly of rounded cubes. *Nature Communications* **2018**, *9* (1), 2228.
52. Savo, R.; Morandi, A.; Müller, J. S.; Kaufmann, F.; Timpu, F.; Reig Escalé, M.; Zanini, M.; Isa, L.; Grange, R., Broadband Mie driven random quasi-phase-matching. *Nature Photonics* **2020**, *14* (12), 740-747.
53. Spinelli, P.; Verschuuren, M. A.; Polman, A., Broadband omnidirectional antireflection coating based on subwavelength surface Mie resonators. *Nature Communications* **2012**, *3* (1), 692.
54. Yang, W.; Xiao, S.; Song, Q.; Liu, Y.; Wu, Y.; Wang, S.; Yu, J.; Han, J.; Tsai, D.-P., All-dielectric metasurface for high-performance structural color. *Nature Communications* **2020**, *11* (1), 1864.
55. Kim, C.; Jung, K.; Yu, J. W.; Park, S.; Kim, S.-H.; Lee, W. B.; Hwang, H.; Manoharan, V. N.; Moon, J. H., Controlled Assembly of Icosahedral Colloidal Clusters for Structural Coloration. *Chemistry of Materials* **2020**, *32* (22), 9704-9712.
56. Liu, T.; VanSaders, B.; Glotzer, S. C.; Solomon, M. J., Effect of Defective Microstructure and Film Thickness on the Reflective Structural Color of Self-Assembled Colloidal Crystals. *ACS Applied Materials & Interfaces* **2020**, *12* (8), 9842-9850.
57. Teh, S.-Y.; Lin, R.; Hung, L.-H.; Lee, A. P., Droplet microfluidics. *Lab on a Chip* **2008**, *8* (2), 198-220.
58. Utada, A. S.; Lorenceau, E.; Link, D. R.; Kaplan, P. D.; Stone, H. A.; Weitz, D. A., Monodisperse Double Emulsions Generated from a Microcapillary Device. *Science* **2005**, *308* (5721), 537-541.
59. Chu, L.-Y.; Utada, A. S.; Shah, R. K.; Kim, J.-W.; Weitz, D. A., Controllable Monodisperse Multiple Emulsions. *Angewandte Chemie International Edition* **2007**, *46* (47), 8970-8974.

60. Zheng, Y.; Yu, Z.; Parker, R. M.; Wu, Y.; Abell, C.; Scherman, O. A., Interfacial assembly of dendritic microcapsules with host–guest chemistry. *Nature Communications* **2014**, *5* (1), 5772.
61. Amstad, E.; Kim, S.-H.; Weitz, D. A., Photo- and Thermoresponsive Polymersomes for Triggered Release. *Angewandte Chemie International Edition* **2012**, *51* (50), 12499-12503.
62. Wang, J.; Mbah, C. F.; Przybilla, T.; Apele Zubiri, B.; Spiecker, E.; Engel, M.; Vogel, N., Magic number colloidal clusters as minimum free energy structures. *Nature Communications* **2018**, *9* (1), 5259.
63. Holtze, C.; Rowat, A. C.; Agresti, J. J.; Hutchison, J. B.; Angilè, F. E.; Schmitz, C. H. J.; Köster, S.; Duan, H.; Humphry, K. J.; Scanga, R. A.; Johnson, J. S.; Pisignano, D.; Weitz, D. A., Biocompatible surfactants for water-in-fluorocarbon emulsions. *Lab on a Chip* **2008**, *8* (10), 1632-1639.
64. Vogel, N.; Utech, S.; England, G. T.; Shirman, T.; Phillips, K. R.; Koay, N.; Burgess, I. B.; Kolle, M.; Weitz, D. A.; Aizenberg, J., Color from hierarchy: Diverse optical properties of micron-sized spherical colloidal assemblies. *Proceedings of the National Academy of Sciences* **2015**, *112* (35), 10845.
65. Chowdhury, M. S.; Zheng, W.; Kumari, S.; Heyman, J.; Zhang, X.; Dey, P.; Weitz, D. A.; Haag, R., Dendronized fluorosurfactant for highly stable water-in-fluorinated oil emulsions with minimal inter-droplet transfer of small molecules. *Nature Communications* **2019**, *10* (1), 4546.
66. Lim, X., Tainted water: the scientists tracing thousands of fluorinated chemicals in our environment. *Nature* **2019**, *566*, 26-30.
67. Manoharan, V. N.; Elsesser, M. T.; Pine, D. J., Dense Packing and Symmetry in Small Clusters of Microspheres. *Science* **2003**, *301* (5632), 483-487.
68. Donaldson, J. G.; Schall, P.; Rossi, L., Magnetic Coupling in Colloidal Clusters for Hierarchical Self-Assembly. *ACS Nano* **2021**, *15* (3), 4989-4999.
69. Stuij, S.; Rouwhorst, J.; Jonas, H. J.; Ruffino, N.; Gong, Z.; Sacanna, S.; Bolhuis, P. G.; Schall, P., Revealing Polymerization Kinetics with Colloidal Dipatch Particles. *Physical Review Letters* **2021**, *127* (10), 108001.
70. Swinkels, P. J. M.; Stuij, S. G.; Gong, Z.; Jonas, H.; Ruffino, N.; Linden, B. v. d.; Bolhuis, P. G.; Sacanna, S.; Woutersen, S.; Schall, P., Revealing pseudorotation and ring-opening reactions in colloidal organic molecules. *Nature Communications* **2021**, *12* (1), 2810.
71. Weiss, J.; Herrmann, N.; McClements, D. J., Ostwald Ripening of Hydrocarbon Emulsion Droplets in Surfactant Solutions. *Langmuir* **1999**, *15* (20), 6652-6657.
72. Yang, Y.; Miller, D. J.; Hawthorne, S. B., Toluene Solubility in Water and Organic Partitioning from Gasoline and Diesel Fuel into Water at Elevated Temperatures and Pressures. *Journal of Chemical & Engineering Data* **1997**, *42* (5), 908-913.
73. Tolls, J.; van Dijk, J.; Verbruggen, E. J. M.; Hermens, J. L. M.; Loeprecht, B.; Schüürmann, G., Aqueous Solubility–Molecular Size Relationships: A Mechanistic Case Study Using C10- to C19-Alkanes. *The Journal of Physical Chemistry A* **2002**, *106* (11), 2760-2765.
74. Demond, A. H.; Lindner, A. S., Estimation of interfacial tension between organic liquids and water. *Environmental Science & Technology* **1993**, *27* (12), 2318-2331.
75. Vialetto, J.; Camerin, F.; Grillo, F.; Ramakrishna, S. N.; Rovigatti, L.; Zaccarelli, E.; Isa, L., Effect of Internal Architecture on the Assembly of Soft Particles at Fluid Interfaces. *ACS Nano* **2021**, *15* (8), 13105-13117.

76. Hanifi, D. A.; Bronstein, N. D.; Koscher, B. A.; Nett, Z.; Swabeck, J. K.; Takano, K.; Schwartzberg, A. M.; Maserati, L.; Vandewal, K.; van de Burgt, Y.; Salleo, A.; Alivisatos, A. P., Redefining near-unity luminescence in quantum dots with photothermal threshold quantum yield. *Science* **2019**, *363* (6432), 1199-1202.
77. Li, Y.; Abolmaali, F.; Allen, K. W.; Limberopoulos, N. I.; Urbas, A.; Rakovich, Y.; Maslov, A. V.; Astratov, V. N., Whispering gallery mode hybridization in photonic molecules. *Laser & Photonics Reviews* **2017**, *11* (2), 1600278.
78. Paik, T.; Diroll, B. T.; Kagan, C. R.; Murray, C. B., Binary and Ternary Superlattices Self-Assembled from Colloidal Nanodisks and Nanorods. *Journal of the American Chemical Society* **2015**, *137* (20), 6662-6669.
79. Cherniukh, I.; Rainò, G.; Sekh, T. V.; Zhu, C.; Shynkarenko, Y.; John, R. A.; Kobiyama, E.; Mahrt, R. F.; Stöferle, T.; Erni, R.; Kovalenko, M. V.; Bodnarchuk, M. I., Shape-Directed Co-Assembly of Lead Halide Perovskite Nanocubes with Dielectric Nanodisks into Binary Nanocrystal Superlattices. *ACS Nano* **2021**, *15* (10), 16488-16500.
80. Montanarella, F.; Geuchies, J. J.; Dasgupta, T.; Prins, P. T.; van Overbeek, C.; Dattani, R.; Baesjou, P.; Dijkstra, M.; Petukhov, A. V.; van Blaaderen, A.; Vanmaekelbergh, D., Crystallization of Nanocrystals in Spherical Confinement Probed by in Situ X-ray Scattering. *Nano Letters* **2018**, *18* (6), 3675-3681.
81. Jishkariani, D.; Elbert, K. C.; Wu, Y.; Lee, J. D.; Hermes, M.; Wang, D.; van Blaaderen, A.; Murray, C. B., Nanocrystal Core Size and Shape Substitutional Doping and Underlying Crystalline Order in Nanocrystal Superlattices. *ACS Nano* **2019**, *13* (5), 5712-5719.
82. Elbert, K. C.; Zygmunt, W.; Vo, T.; Vara, C. M.; Rosen, D. J.; Krook, N. M.; Glotzer, S. C.; Murray, C. B., Anisotropic nanocrystal shape and ligand design for co-assembly. *Science Advances* **2021**, *7* (23), eabf9402, 1-10.
83. Wang, J.; Liu, Y.; Cai, Q.; Dong, A.; Yang, D.; Zhao, D., Hierarchically Porous Silica Membrane as Separator for High-Performance Lithium-Ion Batteries. *Advanced Materials* **2022**, *34* (3), 2107957.
84. Lu, X.; Li, M.; Peng, Y.; Xi, X.; Li, M.; Chen, Q.; Dong, A., Direct Probing of the Oxygen Evolution Reaction at Single NiFe₂O₄ Nanocrystal Superparticles with Tunable Structures. *Journal of the American Chemical Society* **2021**, *143* (41), 16925-16929.
85. Chernomordik, B. D.; Marshall, A. R.; Pach, G. F.; Luther, J. M.; Beard, M. C., Quantum Dot Solar Cell Fabrication Protocols. *Chemistry of Materials* **2017**, *29* (1), 189-198.
86. Voznyy, O.; Levina, L.; Fan, J. Z.; Askerka, M.; Jain, A.; Choi, M.-J.; Ouellette, O.; Todorović, P.; Sagar, L. K.; Sargent, E. H., Machine Learning Accelerates Discovery of Optimal Colloidal Quantum Dot Synthesis. *ACS Nano* **2019**, *13* (10), 11122-11128.
87. Kovalenko, M. V.; Schaller, R. D.; Jarzab, D.; Loi, M. A.; Talapin, D. V., Inorganically Functionalized PbS–CdS Colloidal Nanocrystals: Integration into Amorphous Chalcogenide Glass and Luminescent Properties. *Journal of the American Chemical Society* **2012**, *134* (5), 2457-2460.
88. Jasieniak, J.; Smith, L.; van Embden, J.; Mulvaney, P.; Califano, M., Re-examination of the Size-Dependent Absorption Properties of CdSe Quantum Dots. *The Journal of Physical Chemistry C* **2009**, *113* (45), 19468-19474.
89. Moreels, I.; Lambert, K.; Smeets, D.; De Mynck, D.; Nollet, T.; Martins, J. C.; Vanhaecke, F.; Vantomme, A.; Delerue, C.; Allan, G.; Hens, Z., Size-Dependent Optical Properties of Colloidal PbS Quantum Dots. *ACS Nano* **2009**, *3* (10), 3023-3030.

90. Lignos, I.; Stavrakis, S.; Nedelcu, G.; Protesescu, L.; deMello, A. J.; Kovalenko, M. V., Synthesis of Cesium Lead Halide Perovskite Nanocrystals in a Droplet-Based Microfluidic Platform: Fast Parametric Space Mapping. *Nano Letters* **2016**, *16* (3), 1869-1877.

TOC graphic

